LAWRENCE
LIVERMORE
NATIONAL
LABORATORY

LLNL-JRNL-402853

Bremsstrahlung and Line Spectroscopy of Warm Dense Aluminum Plasma Generated by EUV Free Electron Laser

U. Zastrau, C. Fortmann, R. Faustlin, Th. Bornath, L. F. Cao, T. Doppner, S. Dusterer, E. Forster, S. H. Glenzer, G. Gregori, A. Holl, T. Laarmann, H. Lee, K.-H. Meiwes-Broer, A. Przystawik, P. Radcliffe, R. Redmer, H. Reinholz, G. Ropke, J. Tiggesbaumker, R. Thiele, N. X. Truong, I. Uschmann, S. Toleikis, T. Tschentscher, A. Wierling

April 10, 2008

Physics Review Letters

Disclaimer

This document was prepared as an account of work sponsored by an agency of the United States government. Neither the United States government nor Lawrence Livermore National Security, LLC, nor any of their employees makes any warranty, expressed or implied, or assumes any legal liability or responsibility for the accuracy, completeness, or usefulness of any information, apparatus, product, or process disclosed, or represents that its use would not infringe privately owned rights. Reference herein to any specific commercial product, process, or service by trade name, trademark, manufacturer, or otherwise does not necessarily constitute or imply its endorsement, recommendation, or favoring by the United States government or Lawrence Livermore National Security, LLC. The views and opinions of authors expressed herein do not necessarily state or reflect those of the United States government or Lawrence Livermore National Security, LLC, and shall not be used for advertising or product endorsement purposes.

Bremsstrahlung and Line Spectroscopy of Warm Dense Aluminum Plasma generated by EUV Free Electron Laser

U. Zastrau,[1] C. Fortmann,[2] R. Fäustlin,[3] Th. Bornath,[2] L. F. Cao,[1] T. Döppner,[4] S. Düsterer,[3] E. Förster,[1] S.H. Glenzer,[5] G. Gregori,[6] A. Höll,[2] T. Laarmann,[3] H. Lee,[7] K.-H. Meiwes-Broer,[2] A. Przystawik,[2] P. Radcliffe,[3] R. Redmer,[2] H. Reinholz,[2] G. Röpke,[2] J. Tiggesbäumker,[2] R. Thiele,[2] N.X. Truong,[2] I. Uschmann,[1] S. Toleikis,[3] T. Tschentscher,[3] and A. Wierling[2]

[1]*Institut für Optik und Quantenelektronik, Friedrich Schiller Universität, Max-Wien Platz 1, 07743 Jena*
[2]*Institut für Physik, Universität Rostock, 18051 Rostock, Germany*
[3]*HASYLAB, DESY Hamburg, Notkestrasse 85, 22603 Hamburg, Germany*
[4]*Lawrence Livermore National Laboratory, University of California, P.O. Box 808, Livermore, CA 94551, USA*
[5]*L-399, Lawrence Livermore National Laboratory, University of California, P.O. Box 808, Livermore, CA 94551, USA*
[6]*Clarendon Laboratory, University of Oxford, Parks Road, Oxford OX1 3PU, United Kingdom*
[7]*Department of Physics, University of California, Berkeley, California, CA 94720, USA*

(Dated: March 7, 2008)

We report on the novel creation of a solid density aluminum plasma using free electron laser radiation at 13.5 nm wavelength. Ultrashort pulses of 30 fs duration and 47 μJ pulse energy were focused on a spot of 25 μm diameter, yielding an intensity of $3 \cdot 10^{14}\,\mathrm{W/cm^2}$ on the bulk Al-target. The radiation emitted from the plasma was measured using a high resolution, high throughput EUV spectrometer. The analysis of both bremsstrahlung and line spectra results in an estimated electron temperature of $(30 \pm 10)\,\mathrm{eV}$, which is in very good agreement with radiation hydrodynamics simulations of the laser–target–interaction. This demonstrates the feasibility of exciting plasmas at warm dense matter conditions using EUV free electron lasers and their accurate characterization by EUV spectroscopy.

Warm dense matter (WDM) [1, 2] has drawn increasing interest in recent times because of its role in understanding the convergence between condensed matter and plasma physics. It is found in numerous astrophysical objects [3] and as a transient state in many laboratory research projects, such as shock compression experiments [4], inertial confinement fusion studies [5] and laser excited plasmas [6].

The creation and investigation of WDM, i.e. matter at temperatures between 1 to 100 eV, and densities ranging from $10^{21}\,\mathrm{cm^{-3}}$ to $10^{24}\,\mathrm{cm^{-3}}$, under controlled conditions in a laboratory is a difficult task even though it is commonly accessed in experiments in which one generates a plasma using solid or near-solid density targets. Rapid temporal variations, steep spatial gradients, and uncertain energy sources lead to indecipherable complexity. To deal with this challenge, a few suggestions and efforts have been made before, such as laser-driven shock heating, x-ray heating, and ion heating techniques [4, 7, 8, 9, 10].

WDM is characterized by electron temperatures comparable to the Fermi energy, i.e. the degeneracy parameter $\theta = k_\mathrm{B}T_\mathrm{e}/E_\mathrm{F} \simeq 1$. Secondly, the plasma coupling parameter $\Gamma = Ze^2/4\pi\epsilon_0 k_\mathrm{B}T\,(4\pi n_\mathrm{e}/3)^{1/3}$ is greater or equal to unity, i.e. the inter-particle Coulomb potential energy exceeds the thermal energy; Z is the ion charge and n_e is the electron density [11]. Both, the electrons and the ions exhibit a high degree of correlation, which depends strongly on the plasma temperature and density. Hence, the description of WDM provides a tremendous challenge to many-particle physics.

Both, the theory for ideal plasmas and condensed matter fail in this regime. Classical plasma theory based on expansions of the correlation contributions in powers of the coupling parameter breaks down since $\Gamma \geq 1$. Strong coupling effects among the various species have to be taken into account. On the other hand, the plasma is too hot as to be considered as condensed matter, i.e. expansions in powers of the degeneracy parameter θ also fails. Thus, the precise knowledge of the plasma temperature is of primary importance, since the coupling parameter and the degeneracy parameter scale linearly with T_e, whereas the electron density enters only with powers of 1/3 and 2/3 respectively into these quantities.

In this Letter, we demonstrate the first successful generation of a plasma at WDM conditions using short-pulse EUV radiation delivered by the free electron laser in Hamburg (FLASH) [12, 13, 14]. Furthermore, it is shown that the measurement of EUV bremsstrahlung emission allows the determination of the plasma temperature. In the experiment, FEL pulses of 91.8 eV photon energy (wavelength $\lambda = 13.5$ nm), 30 fs pulse duration, and 47 μJ pulse energy (about $3.2 \cdot 10^{12}$ photons) with a standard deviation of 3 μJ were focused on a 25 μm focal spot under 45° incident angle, reaching an intensity of $3 \cdot 10^{14}\,\mathrm{W/cm^2}$. At the chosen wavelength, the critical density for penetration into the bulk $n_\mathrm{crit} = (2\pi c)^2\epsilon_0 m_\mathrm{e}/e^2\lambda^2 = 6.1 \cdot 10^{24}\,\mathrm{cm^{-3}}$ is about 60 times higher than the solid density $n_\mathrm{solid} \simeq 10^{23}\,\mathrm{cm^{-3}}$.

TABLE I: List of the spectral lines emitted from the plasma, identified with the NIST database [nis].

Experiment data [nm]	NIST data [nm]	Relative intensity (NIST)	Oscillator stregnth f (NIST)	Transition
11.6 ± 0.2	11.646	250	0.332	Al IV: $2s^2 2p^6$ -$2s^2 2p^5 (^2p^0_{1/2}) 4d$
16.2 ± 0.2	16.169	700	0.247	Al IV: $2s^2 2p^6$ -$2s^2 2p^5 (^2p^0_{1/2}) 3s$
17.2 ± 0.2	17.283	–	–	Al III: $2p^6 3p$ -$2p^5 (^2p^0) 3s 3p (3p^0)$

Therefore, energy is deposited deeply into a target volume of $\pi \times (12.5\,\mu\mathrm{m})^2 \times 40\,\mathrm{nm}$, where the number of 10^{12} atoms is in the same order of magnitude as the incident photon number. The FEL was run in multibunch operation mode at 5 Hz repetition rate, with 20 pulses in a bunch. Five separate experiments with an total integrated interaction time of 13.5 min were performed. EUV emission spectra in the region of 6–19 nm were measured with a high throughput transmission grating spectrometer. The sum of all spectra is shown in FIG. 1(a). The main peak at 13.5 nm stems from Rayleigh scattering of the FEL photons by the bound aluminum electrons. Furthermore, spectral lines from Al III and Al IV are observed and identified using the NIST tables [nis] as listed in Tab. I. The continuum background is formed by free-free transition radiation (bremsstrahlung) and free-bound recombination radiation. This continuum is partly reabsorbed. Consequently, the absorption $L_{\mathrm{II/III}}$-edge at 17 nm can be seen even in the FEL-ionized Al-layer, like for laser excited silicon at a similar excitation flux [15].

From the experimental spectra, information about the plasma parameters is obtained. The electron temperature is inferred by analyzing of the continuum background due to bremsstrahlung. We use Kramers' law [16]

$$j_{\mathrm{ff}}(\lambda) = \left(\frac{e^2}{4\pi\epsilon_0}\right)^3 \frac{16\pi Z^2 n_{\mathrm{e}} \mathrm{e}^{-2\pi\hbar c/\lambda k_{\mathrm{B}} T_{\mathrm{e}}}}{3 m_{\mathrm{e}} c^2 \lambda^2 \sqrt{6\pi k_{\mathrm{B}} T_{\mathrm{e}} m_{\mathrm{e}}}}\, g_T(\lambda) \quad (1)$$

for the free-free emissivity $j_{\mathrm{ff}}(\lambda)$ with the mean ion charge Z and the electron mass m_{e}. $g_{\mathrm{T}}(\lambda)$ is the wavelength dependent Gaunt factor [17], accounting for medium and quantum effects. It is calculated in Sommerfeld approximation [18].

FIG. 1(a) shows the experimental data and the bremsstrahlung calculated for three different electron temperatures $k_{\mathrm{B}}T_{\mathrm{e}} = 20, 30$, and 40 eV. The best fit is obtained for 30 eV. Note, that free-bound transitions were not considered in the fits, which explains the deviations between the fit curves and the experimental data, especially in the short wavelength part of the spectrum and for wavelengths larger than 17.0 nm, i.e. the L-edge position. From the height of L-edge, the penetration depth of the EUV radiation into the target can be determined to be 40 nm, using the tabulated opacities found in Ref. [29]. The photon number counts allow to estimate the free electron density, which is compatible with the values obtained from hydrodynamics simulations, see below.

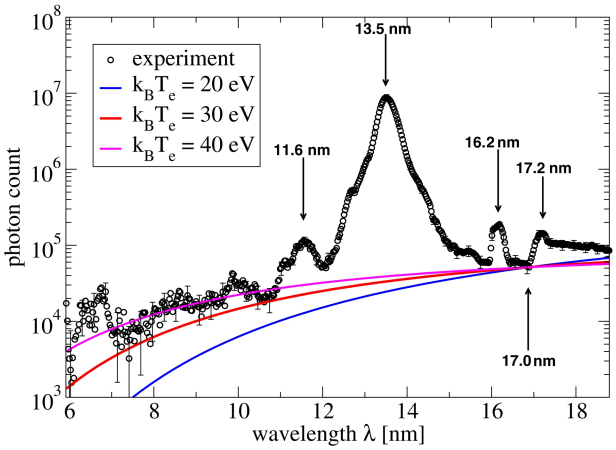

(a)

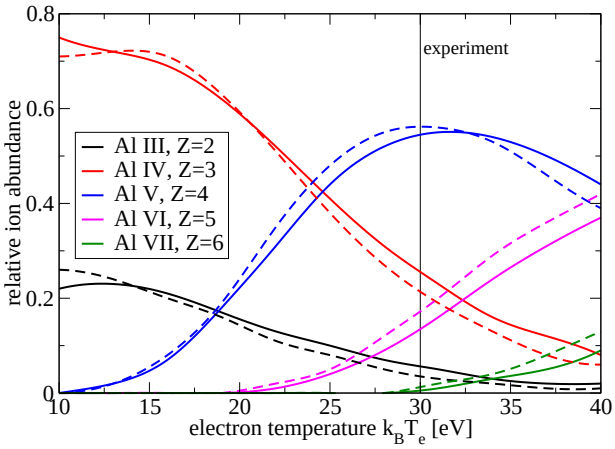

(b)

FIG. 1: (Color online) (a) Measured EUV spectrum from the aluminum plasma (points with error bars, the values were divided by the detection efficiency), and bremsstrahlung calculations for different electron temperatures. (b) Calculation of the relative Al ion species abundance from COMPTRA04 as a function of the electron temperature. Solid line is for Al density $\rho_{\mathrm{Al}} = 2.7\,\mathrm{g/cm^3}$, dashed line: $\rho_{\mathrm{Al}} = 1.5\,\mathrm{g/cm^3}$.

Additionally, the electron temperature can be obtained from the ratio of integrated line intensities for the identified transition lines as follows from the Boltzmann dis-

tribution [19],

$$\frac{I_1}{I_2} = \frac{\omega_1^3}{\omega_2^3}\frac{f_1}{f_2}\mathrm{e}^{-\hbar(\omega_1-\omega_2)/k_\mathrm{B}T_\mathrm{e}} \ , \qquad (2)$$

with the integrated line intensities I_ν, the corresponding photon frequencies ω_ν, and oscillator strengths f_ν. Here, the Al IV lines (doublets) at λ_1=16.1688 nm and λ_2 =11.646 nm are used. The corresponding oscillator strengths are given in Tab. I. The lines were integrated from 15.9 nm to 16.3 nm and from 10.8 nm to 11.9 nm, respectively. The bremsstrahlung background was subtracted before the integration. The resulting temperature is $T_\mathrm{e} = (34 \pm 6)\,\mathrm{eV}$, which is in excellent agreement with the electron temperature obtained from the bremsstrahlung continuum.

The relative abundance of ion species inside aluminum assuming electron temperatures from 10 eV to 40 eV was calculated with the code COMPTRA04 [20], results are shown in FIG. 1(b). The concentration of ion species from the simulation, which used the bremsstrahlung fit temperature, complies with the observed line emission spectrum. At $k_\mathrm{B}T_\mathrm{e} = 30\,\mathrm{eV}$, the ions Al III, Al IV, Al V, and Al VI take the ratios of about 5%, 25%, 55%, and 15%, respectively. Amounts of Al I, Al II, as well as Al VII and higher are negligible. This is consistent with the observation of Al III and Al IV in the measured spectra, see Tab. I. Lines from Al V and Al VI are not visible in the spectrum, since they overlap with the reflected laser light (central peak). Transition lines from Al VII that lie in the observed spectral range have not been found. This coincides with the theoretical result that Al VII is negligible at the present conditions. On the other hand, transition lines from Al VII have previously been observed in optical laser–matter–interaction experiments [21]. This is well understood by looking at the different mechanisms of absorption and ionization in the case of optical light as opposed to the case of EUV photons, where the main absorption mechanism in solid aluminum is photoionization [22].

EUV FEL photons at 92 eV photon energy exceed the $2p$ level binding energy of 72.5 eV and hence dominantly excite $2p$ bound electrons with a photoionization cross-section of $\sigma_\mathrm{PI} = 7\,\mathrm{Mbarn}$ [29]. These photoelectrons have a high excess energy of about 20 eV and excite further atoms by impact ionization, resulting in lower energy electrons. Beside these, there exist also mid-energy Auger electrons. The electrons equilibrate on a timescale of a hundred femtoseconds. [2, 14, 23]. During and after this process, the electron gas transfers its energy to the lattice through electron-phonon scattering on a picosecond timescale, resulting in a significantly lower electron temperature.

This is quite different to the situation of WDM created by optical lasers, where the absorption is due to multi-photon ionization, inverse bremsstrahlung, and collective

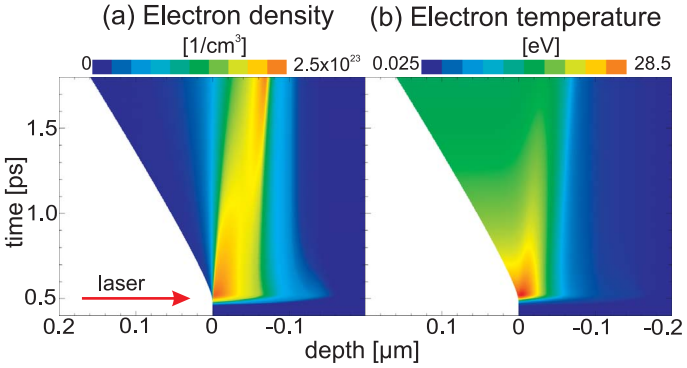

FIG. 2: (Color) HELIOS simulation results for the electron density (right) and electron temperature (left) as a function of time and radius.

and nonlinear processes [24]. Also, when the critical free electron density of the optical laser is reached, most light is reflected and absorption is limited to the skin layer, leaving behind a plasma with steep density and temperature gradients.

In our case of matter interacting with EUV photons, nonlinear absorption is negligible at the considered intensity and resonance absorption is not important since the plasma is undercritical at all stages. Thus, photoexcitation is the dominant absorption mechanism and no "hot" electron production in the keV to MeV range is possible. The refraction index is always close to one, which means refraction in the plasma is negligible. At the very beginning when the EUV pulse reaches the target, the target is a cold solid. The energy deposition process inside the target can be treated in linear approximation, using the tabulated mass absorption coefficients for cold matter [29]. At later times, the absorption coefficient crossection is predicted to decrease slightly [22], because the matter is partially ionized. We conclude that the FEL energy is distributed quite homogeneously throughout the interaction zone.

To illustrate the hydrodynamic processes after the laser–target–interaction and to predict the electron temperature, 1D radiation hydrodynamics simulations using HELIOS [25] have been performed. HELIOS features amongst others a Lagrangian reference frame (i.e., grid moves with fluid), separate ion and electron temperature plasmas and flux-limited Spitzer thermal conductivity. It allows the deposition of laser energy via inverse bremsstrahlung as well as bound-bound and bound-free electron transitions. The simulation results are shown in Fig. 2. Per atom, 2.6 electrons were assumed to be ionized before irradiation, which is the average ionization degree in metallic aluminum. On the timescale of the FEL pulse, both electron density and electron temperature rise homogeneously within the 40 nm thick absorption layer. Near the plasma-vacuum

interface, conditions of $n_e \simeq 10^{22} - 10^{23}\,\mathrm{cm}^{-3}$ and $k_B T_e \leq 28.5\,\mathrm{eV}$ are observed, which agrees with the results for T_e obtained from the spectral analysis above. The simulation shows that these conditions exist a few hundred femtoseconds.
Hydrodynamic plasma expansion as well as electron diffusion to the cold matter of the bulk target and heat conduction will set in after this period. Before this expansion, the created WDM exists and evolves as an isolated state, i.e. the plasma density can be assumed constant and hydrodynamic motion is neglectible [26]. Afterwards, the density will change approximately by a factor of two during the first several picoseconds which influences the relative abundance of ion species only slightly, see Fig. 1(b).

In summary, the generation of WDM by interaction of EUV FEL radiation with a solid aluminum target was demonstrated for the first time. EUV emission spectra yield valuable information about the plasma temperature and composition. The electron temperature was determined by analysis of the line and continuum emission spectra as $k_B T_e = (30 \pm 10)\,\mathrm{eV}$, and the line spectrum shows the presence of Al III and Al IV ions. These results are in perfect agreement with theoretical predictions of the ion species abundance and radiation hydrodynamics modelling. Interestingly, hydrodynamic processes seem to play a minor role for the first hundred femtoseconds after excitation. Our results provide new complementary information to results that were reported in the case of optical laser–matter interaction [21]. Moreover, the generation of WDM in a homogeneous manner, without strong gradients, as in optical laser experiments, is demonstrated opening new possibilities for future research.

Further and detailed studies of WDM will include spatial and temporal dependent observations of its elementary parameters such as electron temperature $T_e(\vec{r}, t)$, electron density $n_e(\vec{r}, t)$, etc. For this regime, novel diagnostic techniques such as x-ray interferometry [27, 28, 29] and x-ray Thomson scattering [30, 31, 32, 33, 34] should be used. In combination with these techniques, the EUV FEL will ignite an unprecedented stage for WDM investigations. This will be important for research of shock physics, applied material studies, planetary interiors, inertial confinement fusion, and other forms of high energy density matter generation.

We thankfully acknowledge financial support by the German Helmholtzgemeinschaft via the Virtual Institute VH-VI-104 and the Deutsche Forschungsgemeinschaft DFG via the Sonderforschungsbereich SFB 652. TL acknowledges financial support from the DFG under Grant No. LA 1431/2-1, RF received DFG funds via GRK 1355. The work of SHG was performed under the auspices of the U.S. Department of Energy by Lawrence Livermore National Laboratory under Contract DE-AC52-07NA27344. SHG was also supported by LDRDs 08-ERI-002, 08-LW-004, and the Alexander-von-Humboldt foundation. The work of GG was partially supported by the Science and Technology Facilities Council of the United Kingdom.

[1] R. W. Lee et al., Laser Part. Beams **20**, 527 (2002).
[2] R. W. Lee et al., J. Opt. Am. B **20**, 770 (2003).
[3] D. Saumon et al., High Pressure Res. **16**, 331 (2000).
[4] L. B. Da Silva et al., Phys. Rev. Lett. **78**, 483 (1997).
[5] T. R. Dittrich et al., Phys. Plasmas **6**, 2164 (1999).
[6] A. Ng et al., Laser Part. Beams **23**, 527 (2005).
[7] T. S. Perry et al., Phys. Rev. E **54**, 5617 (1996).
[8] J. J. MacFarlane et al., Phys. Rev. E **66**, 046416 (2002).
[9] D. H. H. Hoffmann et al., Phys. Plasmas **9**, 3651 (2002).
[10] P. Patel et al., Phys. Rev. Lett. **91**, 125004 (2003).
[11] S. Ichimaru, Rev. Mod. Phys. **54**, 1017 (1982).
[12] Linac Coherent Light Sources (LCLC) Design Study Report SLAC-R-0521 (1998).
[13] in *TESLA Technical Design Report, Part V: The X-ray Free Electron Laser*, edited by G. Materilik and T. Tschentscher (DESY, Hamburg, Germany, 2001), no. 2002-011 in DESY-Report.
[14] T. Tschentscher and S. Toleikis, Eur. Phys. J. D. **36**, 193 (2005).
[nis] URL `http://physics.nist.gov`.
[15] K. Oguri et al., Appl. Phys. Lett. **87**, 011563 (2005).
[16] H. A. Kramers, Philos. Mag. **46**, 836 (1923).
[17] J. A. Gaunt, Proc. R. Soc. A **126**, 654 (1930).
[18] C. Fortmann et al., High Energy Density Physics **2**, 57 (2006).
[29] URL `http://henke.lbl.gov/optical_constants/pert_form.html`.
[19] W. Lochte-Holtgreven, in *Plasma Diagnostics*, edited by W. Lochte-Holtgreven (AIP Press, New York, 1995), p. 135.
[20] S. Kuhlbrodt et al., Contrib. Plasma Phys. **45**, 73 (2005).
[21] U. Teubner et al., Appl. Phys. Lett. **59**, 2672 (1991).
[22] M. Fajardo et al., Eur. Phys. J. D **29**, 69 (2004).
[23] A. L. Dobryakov et al., Physica Scripta **60**, 572 (1999).
[24] P. Gibbon and E. Förster, Plasma Phys. Control. Fusion **38**, 769 (1996).
[25] J. MacFarlane et al., J. Quant. Spectrosc. Radiat. Transfer **99**, 381 (2006).
[26] M. M. Murnane et al., Science **251**, 531 (1991).
[27] L. B. Da Silva, Phys. Rev. Lett. **74**, 3991 (1995).
[28] J. Flevich et al., Opt. Lett. **25**, 356 (2000).
[29] J. Flevich et al., Appl. Opt. **43**, 3938 (2004).
[30] D. Riley et al., Phys. Rev. Lett. **84**, 1074 (2000).
[31] O. L. Landen et al., J. Quant. Spectrosc. Radiat. Transfer **71**, 465 (2001).
[32] A. Höll et al., Eur. Phys. J. D **29**, 169 (2004).
[33] S. H. Glenzer et al., Phys. Rev. Lett. **98**, 065002 (2007).
[34] A. Höll et al., High Energy Density Physics **3**, 120 (2007).